

# Application of a physically-based model to forecast shallow landslides occurrence at regional scale

Teresa Salvatici<sup>1</sup>, Veronica Tofani<sup>1</sup>, Guglielmo Rossi<sup>1</sup>, Michele D'Ambrosio<sup>1</sup>, Carlo Tacconi Stefanelli<sup>1</sup>, Elena Benedetta Masi<sup>1</sup>, Ascanio Rosi<sup>1</sup>, Veronica Pazzi<sup>1</sup>, Pietro Vannoci<sup>1</sup>, Miriana Petrolo<sup>1</sup>, Filippo Catani<sup>1</sup>, Sara Ratto<sup>2</sup>, Hervé Stevenin<sup>2</sup> and Nicola Casagli<sup>1</sup>

<sup>1</sup>Department of Earth Sciences, University of Firenze, Firenze, 50121, Italy

<sup>2</sup>Centro funzionale, Regione Autonoma Valle d'Aosta, Aosta, 11100, Italy

Correspondence to: Michele D'Ambrosio (michele.dambrosio@unifi.it)

## Abstract.

In this work, we apply a physically-based model, namely the HIRESSS (High REsolution Stability Simulator) model, to forecast the occurrence of shallow landslides at regional scale. HIRESSS is a physically based distributed slope stability simulator for analysing shallow landslide triggering conditions during a rainfall event. The software is made of two parts: hydrological and geotechnical. The hydrological model is based on an analytical solution of an approximated form of the Richards equation while the geotechnical stability model is based on an infinite slope model that takes into account the unsaturated soil condition. The test area is a portion of the Valle d'Aosta region, located in North-West Alpine mountain chain. The geomorphology of the region is characterized by steep slopes with elevations ranging from 400 m a.s.l. of Dora Baltea's river floodplain to 4810 m a.s.l. of Mont Blanc. In the study area, the mean annual precipitation is about 800-900 mm. These features lead to the territory to be very prone to landslides, mainly shallow rapid landslides and rock falls. In order to apply the model and to increase its reliability, an in-depth study of the geotechnical and hydrological properties of hillslopes controlling shallow landslides formation was conducted. In particular, two campaigns of on site measurements and laboratory experiments were performed with 12 survey points. The data collected contributes to generate input map of parameters for HIRESSS model. In order to consider the effect of vegetation on slope stability, the soil reinforcement due to the presence of roots has been also taken into account based on vegetation maps and literature values of root cohesion. The model was applied in back analysis on two past events that have affected Valle d'Aosta region between 2008 and 2009, triggering several fast shallow landslides. The validation of the results, carried out using a database of past landslides, has provided good results and a good prediction accuracy of the HIRESSS model both from temporal and spatial point of view.

## 1 Introduction

Landslide prediction at regional scale can be performed following two approaches: a) rainfall thresholds based on statistical analysis of rainfall and landslides and b) physically-based deterministic models. While the first approach is currently extensively used at regional scale (Aleotti, 2004; Cannon et al., 2011; Martelloni et al., 2012; Rosi et al., 2012; Lagomarsino et al., 2013), the latter is more frequently applied at slope or catchment scale (Dietrich and Montgomery 1998; Pack et al. 2001; Baum et al. 2002, 2010; Lu and Godt 2008; Simoni et al. 2008; Ren et al. 2010; Arnone et al. 2011; Salciarini et al., 2012; Park et al., 2013; Rossi et al. 2013; Salciarini et al. 2017). The poor knowledge of hydrological and geotechnical parameters spatial distribution, caused by the extreme heterogeneity and inherent variability of soil at large scale (Mercogliano et al., 2013; Tofani et al., 2017), mainly avoid the physically-based model application at regional scale. On the other hand, physically-based models allow to predict spatially and

temporally the occurrence of landslides with high accuracy producing accurate hazard maps that can be of help for landslide risk assessment and management.

In this work, we apply the physically based model, named HIRESSS (Rossi et al., 2013) in Eastern part of Valle d'Aosta region (Italy), in North-West Alpine mountain chain in order to test the capacity of the model to forecast the occurrence of shallow landslides at regional scale. In particular, the objectives of the work are: i) to properly characterise the geotechnical and hydrological parameters of the soil to feed the HIRESSS model and to spatialize this punctual information in order to have spatially-continuous maps of the model input data ii) to test the HIRESSS code for two selected rainfall events that have triggered several shallow landslides and to validate the model results. HIRESSS is a physically based distributed slope stability simulator for analysing shallow landslide triggering conditions in real time and in large areas using parallel computational techniques. In the area selected, an in-depth study of the geotechnical and hydrological properties of hillslopes controlling shallow landslides formation was conducted, performing two campaigns (12 survey points) of in-situ measurements and laboratory tests. Furthermore, the HIRESSS model has been modified to take into account the effect of the root reinforcement to the stability of slopes based on plant species distribution and literature values of root cohesion.

## 2 Study area and rainfall events

The study area, called alert Zone B by the regional civil protection authorities, is located in eastern part of Valle d'Aosta region, in North-West Alpine mountain chain (Fig. 1). The area is characterized by three main valleys: Champorcher valley, Gressoney or Lys valley, and Ayas valley. The first is located on the right side of Dora Baltea water catchment, and represents the southern part of the study area. The second and third valleys show N-S orientation, and they are delimited to north by Monte Rosa massif (4527 m a.s.l) and to south by Dora Baltea river.

From a geological point of view, the Valle d'Aosta is located NW with respect to the Insubrica Line, in particular, there are three systems of Europa chain: the Austroalpino, the Pennidiche and the Elvetico-Ultraelevato systems (De Giusti, 2004). Fig. 2 shows the lithological map of the study area obtained by reclassifying the geological units according to 11 lithological groups: landslides, calcareous schist, alluvial deposits, glacial deposits, colluvial deposits, glacier, granites, mica schists, green stone, black schists and serpentinites. In detail in the study area the main lithologies outcropping are metamorphic and intrusive rocks, in particular granites, metagranites, schists and serpentinite.

The geomorphology of the region is characterized by steep slopes and valleys shaped by glaciers. The glacial modelling is shown in the U-shaped of Lys and Ayas valleys, and the erosive depositional forms found in the Ayas valley. The three valleys' watercourses, the Lys creek, the Evançon creek, and the Dora Baltea river, contributed to the glacial deposits modelling with the formation of alluvial fans. The climate of the region is characterized by high variability strongly influenced by altitude (ranging from 400 m a.s.l of Dora Baltea's river floodplain to 4810 m a.s.l. of Mont Blanc), with a continental climate in the valleys floor and an Alpin climate at high altitudes.

The slope steepness, together with mean annual precipitation of 800-900 mm are the main landslide triggering factors. These features lead the study area to be prone to landsliding, in particular rock falls, deep seated gravitational slope deformations (DSGSD), rocks avalanches, debris avalanches, debris flows, and debris slides (Catasto dei Dissesti Regionale – form Val d'Aosta Regional Authorities). In this work we model the triggering conditions of shallow landslides, i.e. soil slips and translational slides and we do not take into account the other types of movement.

The HIRESSS model simulated two past events, one in 2008 and one in 2009, and the validation of the model performance was carried out comparing the results with the landslide regional database.

In particular:



- 24 - 31 May 2008: on 28 and 29 May 2008 intense and persistent rainfall was recorded across the Valle d'Aosta region with a total precipitation in the study area of about 250 mm causing flooding, debris flows and rockfalls.
- 25 - 28 April 2009: from 26 April to 28 April 2009 heavy rainfall affected the south-eastern part of the Valle d'Aosta region, with the highest precipitation recorded at the Lillianes Granges station of about 268 mm. This precipitation triggered several landslides.

### 3 Methodology

#### 3.1 HIRESSS description

The physically-based distributed slope stability simulator HIRESSS (Rossi et al., 2013) is a model developed to analyse shallow landslide triggering conditions on large scale at high spatial and temporal resolution using parallel calculation method. Two parts compose the model: hydrological and geotechnical (Rossi et al., 2013). The hydrological part is based on a dynamical input of the rainfall data which are used to calculate the pressure head and provide it to the geotechnical stability model. The hydrological model is initiated as a modelled form of hydraulic diffusivity, using an analytical solution of an approximated form of the Richards equation under the wet condition (Richards, 1931). The equation solution allows us to calculate the pressure head variation ( $h$ ), depending on time ( $t$ ) and depth of the soil ( $Z$ ). The solutions are obtained by imposing some boundary conditions as described by Rossi et al. (2013).

The geotechnical stability model is based on an infinite slope stability model. The model considers the effect of matric suction in unsaturated soils, taking into account the increase in strength and cohesion. The stability of slope at different depths ( $Z$  values) is computed since the hydrological model calculates the pressure head at different depths. The variation of soil mass caused by water infiltration on partially saturated soil is also modelled. The original FS equations (Rossi et al., 2013) were modified taking into account the effect of root reinforcement ( $c_r$ ) as an increase of soil cohesion ( $c'$ ) according to the Eq. 1:

$$c_{tot} = c' + c_r \quad (1)$$

Regarding the geotechnical influence of roots on the soil strength, roots seem to affect the cohesion parameter only, while the friction angle would be poorly or not at all interested by reinforcement (Waldron and Dakessian, 1981; Gray and Ohashi 1983; Operstein and Frydaman, 2000; Giadrossich et al., 2010). Therefore, is necessary to consider the root cohesion in calculating FS and consequently in applying HIRESSS model.

The root reinforcement (or root cohesion) can be considered equal to (Eq. 2):

$$c_r = kT_r(A_r/A) \quad (2)$$

where  $T_r$  is the root failure strength (tensile, frictional, or compressive) of roots per unit area of soil,  $A_r/A$  the root area ratio (proportion of area occupied by roots per unit area of soil),  $k$  a coefficient dependent on the effective soil friction angle and the orientation of roots. The measure of  $c_r$  varies with vegetal species, within a single species depends on how plants respond to environmental characteristics and fluctuations.

The new equation of FS at unsaturated conditions is therefore (Eq. 3):

$$FS = \frac{\tan \varphi}{\tan \alpha} + \frac{c_{tot}}{\gamma_d y \sin \alpha} + \frac{\gamma_w h \tan \varphi \left[ 1 + (h_b^{-1} |h|)^{\lambda+1} \right]^{\frac{\lambda}{\lambda+1}}}{\gamma_d y \sin \alpha} \quad (3)$$

where  $\varphi$  is the friction angle,  $\alpha$  is the slope angle,  $\gamma_d$  is the dry soil unit weight,  $y$  is the depth,  $\gamma_w$  is the water unit weight,  $h$  is the pressure head,  $h_b$  is the bubbling pressure, and  $\lambda$  is the pore size index distribution. In saturated condition the equation of FS (Rossi et al., 2013) becomes (Eq. 4):

$$FS = \frac{\tan \varphi}{\tan \alpha} + \frac{c_{tot}}{(\gamma_d(y-h) + \gamma_{sat}h) \sin \alpha} - \frac{\gamma_w h \tan \varphi}{(\gamma_d(y-h) + \gamma_{sat}h) \tan \alpha} \quad (4)$$

where  $\gamma_{sat}$  is the saturated soil unit weight.

One of the major problems, associated with the deterministic approach employed on a large scale, is the uncertainty of the static input parameters or geotechnical parameters of the soil. The method used for the estimation of parameters spatial variability is the Monte Carlo Simulation. The Monte Carlo simulation achieves a probability distribution of input parameters providing results in terms of slope failure probability (Thiery et al. 2017). The developed software uses the computational power offered by multicore and multiprocessor hardware, from modern workstations to supercomputing facilities (HPC), to achieve the simulation in reasonable runtimes, compatible with civil protection real time monitoring (Rossi et al. 2013). The HIRESSS model loads spatially distributed data arranged as 12 input raster maps and the maps of rainfall intensity. These input raster maps are: slope gradient; effective cohesion ( $c'$ ); root cohesion ( $c_r$ ); friction angle ( $\varphi'$ ); dry unit weight ( $\gamma_d$ ); soil thickness; hydraulic conductivity ( $k_s$ ); initial soil saturation ( $S$ ); pore size index ( $I$ ); bubbling pressure ( $h_s$ ); effective porosity ( $n$ ); and residual water content ( $q_r$ ). and rainfall intensity.

### 3.2 HIRESSS input data preparation

The input parameters can be divided in two classes: the static data and the dynamical data. Static data are geotechnical and morphological parameters while the dynamical data is represented by the hourly rainfall intensity. Static data are read only once at the beginning of the simulation while dynamical inputs are continuously updated.

The HIRESSS input are in raster, therefore point data and parameters have to be adequately spatially distributed. In this application the spatial resolution was 10 m.

#### Static data

The slope gradient was calculated from the DEM (Digital Elevation Model- 2006). Effective cohesion, friction angle, hydraulic conductivity, effective porosity and dry unit weight, were obtained, spatializing according to lithology, the soil punctual parameters derived from the in situ and laboratory geotechnical tests and analysis.

In particular, the properties of slope deposits were determined by in situ and laboratory measurements (Bicocchi et al., 2016; Tofani et al., 2017) at 12 survey points. To carry out the in situ tests the survey points were selected following these characteristics: i) physiography, ii) landslides occurrence, and iii) geo-lithology (Fig. 2). Regarding the first point, a high-resolution DEM (from Val d'Aosta Regional Authorities) together with a careful first surveys were used to locate the most suitable slopes. The surveys took place in two sessions, the first one in August 2016, and the second one in September 2016. The following analyses were conducted:

- registration of geographical position using a GPS and photographic documentation of the site characteristics (morphology and vegetation);
- in situ measurement of saturated hydraulic conductivity ( $k_s$ ) by means of the constant-head well permeameter Amoozometer;
- sampling of an aliquot (~2 kg each) of the material for laboratory tests, including grain size distributions, index properties, Atterberg limits and direct shear tests.

The permeability in-situ measurements and the soil samplings were made at depth ranging from 0.4 to 0.6 m below the ground level. The evaluation of the  $k_s$  (saturated hydraulic conductivity or permeability) was made with the *Amoozometer* permeameter (Amoozegar, 1989). The measurement was obtained by observing the amount of water required to maintain a constant volume of water into the hole. In situ measurements are then applied into the Glover solution (Amoozegar, 1989). which calculates the saturated permeability of the soils. The  $k_s$  is a very useful parameter not only for slope stability modelling but also for many other hydrological problems (groundwater, surface water runoff and sub-surface, flow calculation of water courses).

In addition, the in situ collected samples were examined in the laboratory to define a wide range of parameters to characterize more extensively the deposits. In particular, the following tests were performed in order to classify the analysed soils:

- grain size distribution (determination of granulometric curve for sieving and settling following ASTM recommendations), and classification of soils (according to AGI and USCS classification, Wagner, 1957);
- determination of the main index properties (porosity, relationships of phases, natural water content  $w_n$ , natural and dry unit weight  $\gamma$  and  $\gamma_d$ ) following the ASTM recommendations;
- determination of Atterberg limits (liquid limit LL, plastic limit PL, and plasticity index PI);
- direct shear test on selected samples.

Soil thickness was calculated by the GIST model (Catani et al., 2010; Del Soldato et al, 2016). Soil characteristic curves parameters (pore size index, bubbling pressure, and residual water content) were derived from literature values (Rawls et al., 1982).

Root cohesion variations in the area (at the soil depth chosen for the physical modelling with HIRESSS) were obtained firstly, identifying the plant species and determining their distribution from *in situ* observations and vegetational maps (Carta delle serie di vegetazione d'Italia, Italian Ministry of the Environment and Protection of Land and Sea). Then, the measure of cohesion due to the presence of roots was assigned to each subarea according to the dominant plant species and literature root cohesion for that species (Bischetti, 2009; Burylo et al., 2010; Vergani et al., 2013) that were calculated considering the Fiber Bundle Model (Pollen et al., 2004). The measure of  $c_r$  varies with vegetal species, within a single species depends on how plants respond to environmental characteristics and fluctuations, so map of root cohesion variations obtained as mentioned is a simplification of reality. This is a necessary simplification as the known methods to evaluate root cohesion variations are not suitable for wide areas and acceptable measurement times.

The last static input data, in this case of study, is the exposure rock mask. This was defined considering the lithological and land use maps, so that HIRESSS model avoided the simulation on steep rock slopes areas.

The geotechnical properties and root cohesion of the soils have been spatialized with respect to a lithological classification.

For each lithological class and plant species the mean value has been selected in order to obtain the HIRESSS input raster parameters.

### 193 Dynamic data

194 In the study area, the rainfall hourly data from 27 pluviometers were available, therefore it was necessary to spatially  
195 distribute them to generate 10x10 m cell size input raster to ensure the correct program operation. The rainfall data were  
196 elaborated applying the Thiessen's polygon methodology (Rhynsburger, 1973) modified to take into account the  
197 elevation. Thiessen's polygon methodology, in fact, allows us to divide a planar space in some regions, and to assign the  
198 regions to the nearest point feature. This approach defines an area around a point, where every location is nearer to this  
199 point than to all the others. Thiessen's polygon methodology do not consider the morphology of the area, so the alert  
200 Zone B was divided in three catchment areas and the polygons were calculated for each rain gauges considering the  
201 reference catchment basin (Fig. 3).

## 202 **4 Results**

203 The results of the geotechnical and hydrological characterization of the soils of the 12 survey points are shown in Table  
204 1 for all survey sites.

205 The results of granulometric tests shown that the analysed soils are predominantly sands with silty gravel (Fig. 4 and  
206 Table 1). Regarding the index properties, the natural soil water content values were predominantly about 20% by  
207 weight, with a maximum and minimum values of 5.1% and 26.2%, respectively. These values reflect their different  
208 ability to hold water in their voids. The measured natural unit weight ( $\gamma$ ) was variable between 15.3 kN/m<sup>3</sup> and 21.7  
209 kN/m<sup>3</sup>, depending not only on the different grain size distribution but also by different thickening and consolidation  
210 states. Regarding saturated unit weight ( $\gamma_{sat}$ ) the measured values range between 18.2 kN/m<sup>3</sup> and 21.5 kN/m<sup>3</sup> (Table 1).

211 The Atterberg limits (LL and PL) were measured on samples with a sufficient passing fraction (> 30% by weight)  
212 through 40 ASTM (0.425 mm) sieve. For sandy prevalent samples, LL values are predominantly around 40% of water  
213 content (% by weight), while the PL is around 30% (Table 1).

214 The effective friction angle varies between a minimum of 25.6° and a maximum of 34.3°, while the effective cohesion  
215 ranges from a minimum of 0.0 kPa to a maximum of 9.3 kPa. Consistent with the presence of sandy soils, the saturated  
216 permeability values were around a medium-high value of 10<sup>-6</sup> m/s. The minimum and maximum values were found  
217 between 1.36·10<sup>-7</sup> m/s and 1.54·10<sup>-5</sup> m/s. Considering the poor variability of samples, the permeability values were  
218 relatively homogeneous and in accordance with the values reported in the literature (Table 1).

219 The additional cohesion induced by roots assumes different values not only depending on plant species and  
220 environmental characteristics, but also on depth of soil, as roots diameter and density vary with latter. Because of such  
221 evidence, studies on roots cohesion of different species report values as function of depth of soil. In the area of the case  
222 study, soils have thinner thickness than those ones in which these studies are carried out. In such thin soils, root systems  
223 organize their growth depending on available space not reaching the same depth of roots of thick soils. Consequently, in  
224 this context root cohesion of species at the different depth is dissimilar related to literature values. Considering this,  
225 map for variation of root cohesion is processed taking for each species the minimum cohesion (among those specified  
226 for each species at the different depth) reported in literature. By doing this, contribution of vegetation to stability of  
227 slopes is considered in FS calculate and at the same time, it is avoided an overestimate of root cohesion.

228 In the area, root cohesion defined as mentioned above ranges from a minimum of 0.0 kPa (mainly in the outcrop area)  
229 to maximum of 8.9 kPa (area occupied by mountain maple on the left bank of river Dora Baltea).

230 In Table 2, the mean values of each input parameters respect to lithological class were reported.

231 The pore size index, bubbling pressure and residual water content are constant in whole area of: 0,322 (-); 0,1466 m and  
232 0,041 (-), respectively.

233 The distributed soil parameters maps are shown in Fig. 5.  
234 The results of rainfall data elaborated using Thiessen's polygon methodology are 192 and 96 rainfall hourly maps for  
235 the 2008 and 2009 event, respectively. In Fig. 6 are reported the cumulative maps of each event.  
236 All these data have been inserted in the HIRESSS model to obtain day-by-day maps of landslide occurrence probability.  
237 The main characteristics of simulation are showed in Table 3. Before to discuss the model results is necessary to check  
238 false positive for both the simulated events, the first day of simulation, characterized by the absence of rainfall, was  
239 analysed. The results showed that those pixels with a high landslide occurrence probability are unstable because of  
240 morphometric reasons, predominantly high slope angles. To remove these false positive, a numeric mask was applied.  
241 Using the GIS software commands, it was possible to calculate the number of pixels of the first simulation day with a  
242 trigger probability value greater than 80% and delete them (Fig. 7). The mask was then applied to the rest of landslide  
243 occurrence probability maps. The resulting maps for each days of the simulated events are shown in the Fig. 8 and Fig.  
244 9.

## 245     **5 Discussion**

246 A back analysis was carried out to evaluate the model performance from a temporal and spatial point of view. To  
247 perform a solid validation is necessary to have information on spatial and temporal location of landslides. In particular,  
248 the time of occurrence is very rarely known with hourly precision, and usually landslides are related to a rainstorm,  
249 without any more precise information on time of occurrence (Rossi et al., 2013). Concerning the spatial landslides  
250 locations, in many cases they are included in the database only as points without any information on the area involved.  
251 In our database, provided by the local authorities, landslides are points with information on the day of occurrence.  
252 In general, for both events temporal validation shows that the daily highest probability of occurrence, computed by  
253 HIRESSS, correspond with the days with real landslide occurrence and with the most intense precipitation.  
254 The results of the first simulated event (24 - 31 May 2008) are shown in Fig. 8. The failure probability in the whole area  
255 is negligible for the first four days (from 24 to 27 May 2008) (Fig. 8a). The rainfall intensity increased since 27 May,  
256 reaching the highest value on 29 May, when the precipitation value was around 100 mm in the eastern sector of study  
257 area.  
258 The HIRESSS model well simulate this passage: the 28 May and 29 May 2008 landslide occurrence probability maps  
259 show a considerable increase of the probability of failure with maximum values around 90% at the East of alert Zone B  
260 (Fig. 8 b, c). In the following days rainfall intensity decreases, and also the probability slowly decreases, being anyway  
261 still high on 30 May 2008. Landslides reported in the database are dated 30 May and 31 May 2008 (Fig. 8d).  
262 Concerning the second event (25 - 28 April 2009) landslide occurrence probability is negligible for the first two days  
263 (25 and 26 April 2009) in the whole area (Fig. 9 a, b), because of the low rainfall intensity. From 27 April 2009 rainfalls  
264 become more intense, especially in the southeast sector of the region, where the cumulated rainfall average was about  
265 151 mm. This event led to many landslides triggered during these days (as reported in the database). Also the  
266 probability maps show high values during these days (Fig. 9 c, d).  
267 In Table 4 the results over 75% of slope failure probability for both events are highlighted and confirm the correct  
268 temporal occurrence of landslides.  
269 The temporal validation was also carried out considering daily cumulative rainfall compared to the landslide failure  
270 probability. In particular, a median of landslide occurrence probability was calculated for four pluviometric areas  
271 identified by Thiessen's polygons methodology, modified according to limits of river basins, both for the event of May

272 2008 and for the April 2009 event (Fig. 10 a, b). As it could be expected, the results show that when the highest rainfall  
273 intensity is measured, the highest probability of occurrence is computed for the all areas and for both events.

274

275 Spatial validation was performed following a pixel by pixel method: this method is the most complex since it consists in  
276 comparing the probability of instability of each pixel with the pixels involved in the actual event that occurred. This  
277 validation implies a great deal of uncertainty in the results since the reports of landslide events may have errors on the  
278 precise spatial location and on the size of the phenomenon. To overcome this problem and taking into account probable  
279 errors caused by the actual spatial location in the database, an area of 1 km<sup>2</sup> (called influence area) around the point of  
280 the landslide were considered in the validation analysis. Inside the influence area, pixels that have the 75% of  
281 probability of failure were considered instable.

282 Figure 11 shows an example of landslide event occurred in the Arnad municipality on 30 May 2008. The model  
283 computes a low failure probability on 24 May 2008 and an increase of probability on 30 May 2008. In Fig. 11a and b it  
284 is possible to note that inside the red circle the red and yellow area increase on 30 May with respect to 24 May. In this  
285 case, the model is able to identify correctly such movement. To better highlight this validation, Figure 10c shows the  
286 number of pixels above 75% of probability calculated by the model, within the circular area of about 1 km<sup>2</sup> around the  
287 all landslides occurred during the event of 2008. For some of the reported landslide events, the number of pixels above  
288 75% increases on 30 May, 2008, only in case of the Champdepraz and Montjovet 2 events the probability does not  
289 increase. This may be caused by the low precision of location of the reported landslide, and maybe because some of the  
290 real landslides reported are other types of movements (rockfalls, rotational slides) that cannot simulated by the  
291 HIRESSES model.

## 292 **6 Conclusion**

293 The HIRESSES code (a physically-based distributed slope stability simulator for analysing shallow landslide triggering  
294 conditions in real time and in large areas) was applied to the eastern sector of Valle d'Aosta region in order to test its  
295 capability to forecast shallow landslides at regional scale. The model was applied in back analysis to two past rainfall  
296 events that have triggered in the study areas several shallow landslides between 2008 and 2009. In order to run the  
297 model and to increase its reliability, an in-depth study of the geotechnical and hydrological properties of hillslopes  
298 controlling shallow landslides formation was conducted. In particular, two campaigns of on site measurements and  
299 laboratory experiments were performed with 12 survey points. The data collected contributes to generate input map of  
300 parameters for HIRESSES model according to lithological classes. The effect of vegetation on slope stability in terms of  
301 root reinforcement has been also taken into account based on the plant species distribution and literature values of root  
302 cohesion to product a map of root reinforcement of the study area. The outcomes of the model are daily failure  
303 probability maps with a spatial resolution of 10 m. To evaluate the model performance both temporal and spatial  
304 validation were carried out, and in general for both the simulated events the computed highest daily probability of  
305 occurrence corresponds to the days and the areas of real landslides.

## 306 **References**

### 307 **Reference List**

308 Aleotti, P.: A warning system for rainfall-induced shallow failures, Eng. Geol., 73, 247–265, doi:10.1016/j.enggeo.2004.01.007,  
309 2004.



310 Amoozegar, A.: Compact constant head permeameter for measuring saturated hydraulic conductivity of the vadose zone, *Soil Sci.*  
311 *Soc. Am. J.*, 53, 1356–1361, 1989.

312 Arnone, E., Noto, L. V., Lepore, C., and Bras, R. L.: Physically- based and distributed approach to analyse rainfall-triggered land-  
313 slides at watershed scale, *Geomorphology*, 133, 3–4, 121–131, 2011.

314 Baum, R., Savage, W., and Godt, J.: Trigrs: A FORTRAN program for transient rainfall infiltration and grid-based regional slope-  
315 stability analysis, Open-file Report, US Geol. Survey, 2002.

316 Baum, R. L. and Godt, J. W.: Early warning of rainfall-induced shallow landslides and debris flows in the USA, *Landslides*, 7, 259–  
317 272, 2010.

318 Bicocchi, G., D'Ambrosio, M., Rossi, G., Rosi, A., Tacconi Stefanelli, C., Segoni, S., Nocentini, M., Vannocci, P., Tofani, V.,  
319 Casagli N., and Catani, F.: Geotechnical in situ measures to improve landslides forecasting models: A case study in Tuscany (Central  
320 Italy), *Landslides and Engineered Slopes, Experience, Theory and Practice*, 2, 419–424, 2016.

321 Bischetti, G. B., Chiaradia, E. A., and Epis, T.: Prove di trazione su radici di esemplari di piante pratiarmati, Rapporto interno,  
322 Istituto di Idraulica Agraria, Università degli Studi di Milano, 2009.

323 Burylo, M.: Relations entre les traits fonctionnels des espèces végétales et leurs fonctions de protection contre l'érosion dans le  
324 milieu marneux restaurés de montagne, Dissertation, University of Grenoble, France, 2010.

325 Cannon, S. H., Boldt, E. M., Laber, J. L., Kean, J. W., and Staley, D. M.: Rainfall intensity–duration thresholds for postfire debris-  
326 flow emergency-response planning, *Nat. Hazards*, 59, 209–236, 2011.

327 Catani, F., Segoni, S., and Falorni, G.: An empirical geomorphology-based approach to the spatial prediction of soil thickness at  
328 catchment scale, *Water Resour. Res.*, 46, W05508, doi:10.1029/2008WR007450, 2010.

329 De Giusti, F., Dal Piaz, G. V., Massironi, M., and Schiavo, A.: Carta geotettonica della Valle d'Aosta alla scala 1:150.000, *Mem. Sci.*  
330 *Geol.*, 55, 129–149, 2004.

331 Del Soldato, M., Segoni, S., De Vita, P., Pazzi, V., Tofani, V., and Moretti, S.: Thickness model of pyroclastic soils along mountain  
332 slopes of Campania (southern Italy), In: Aversa, et al. (Eds.), *Landslides and Engineered Slopes, Experience, Theory and Practice*,  
333 Associazione GEotecnica Italiana, Rome, Italy, 797–804, 2016.

334 Dietrich, W. and Montgomery, D.: Shalstab: a digital terrain model for mapping shallow landslide potential, NCASI (National Coun-  
335 cil of the Paper Industry for Air and Stream Improvement) Technical Report, February, 1998.

336 Giadrossich, F., Preti, F., Guastini, E., and Vannocci, P.: Metodologie sperimentali per l'esecuzione di prove di taglio diretto su terre  
337 rinforzate con radici, *Experimental methodologies for the direct shear tests on soils reinforced by roots, Geologia tecnica &*  
338 *ambientale*, 4, 5–12, 2010.

339 Gray, D. H., and Ohashi, H.: Mechanics of fiber reinforcement in sand, *J. Geotech. Eng.*, 109, 335–353, 1983.

340 Lagomarsino, D., Segoni, S., Fanti, R., and Catani, F.: Updating and tuning a regional scale landslide early warning system, *Land-*  
341 *slides*, 10, 91–97, 2013.

342 Lu, N. and Godt, J. W.: Infinite-slope stability under steady un- saturated seepage conditions, *Water Resour. Res.*, 44, W11404,  
343 doi:10.1029/2008WR006976, 2008.

344 Martelloni, G., Segoni, S., Fanti, R., and Catani, F.: Rainfall thresh- olds for the forecasting of landslide occurrence at regional scale,  
345 *Landslides*, 9, 485–495, 2012.

346 Mercogliano, P., Segoni, S., Rossi, G., Sikorsky, B., Tofani, V., Schiano, P., Catani, F., and Casagli, N.: Brief communication “A  
347 prototype forecasting chain for rainfall induced shallow landslides”, *Nat. Hazards Earth Syst. Sci.*, 13, 771–777, doi:10.5194/nhess-  
348 13-771-2013, 2013.

349 Operstein, V., and Frydman, S.: The influence of vegetation on soil strength, *Ground. Improv.*, 4, 81–89, 2000.

350 Pack, R. T., Tarboton, D. G., and Goodwin, C. N.: Assessing terrain stability in a gis using sinmap, in “15th Annual GIS Conference,  
351 GIS 2001, Vancouver, British Columbia, Canada, 2001.

352 Park, H. J., Lee, J. H. and Woo, I.: Assessment of rainfall-induced shallow landslide susceptibility using a GIS-based probabilistic  
353 approach, *Eng. Geol.*, 161, 1–15, 2013.

354 Pollen, N., Simon, A., and Collison, A. J. C.: Advances in assessing the mechanical and hydrologic effects of riparian vegetation on  
355 streambank stability, in *Riparian Vegetation and Fluvial Geomorphology*, *Water Sci. Appl. Ser.*, 8, edited by Bennett, S., and Simon,  
356 A., AGU, Washington, D. C., 125–139, 2004.

357 Rawls, W. J., Brakensiek, D. L., and Saxton K. E.: Estimating soil water properties, *Transactions, ASAE*, 25(5), 1316–1320 and 1328  
358 1982.

359 Ren, D., Fu, R., Leslie, L. M., Dickinson, R. and Xin X.: A storm-triggered landslide monitoring and prediction system: formulation  
360 and case study, *Earth Interact.*, 14, 1–24, 2010.

361 Rhynsburger, D.: Analytic delineation of Thiessen polygons, *Geogr. Anal.*, 5(2), 133–144, 1973.

362 Richards, L. A.: Capillary conduction of liquids through porous mediums, PhD Thesis, Cornell University, 1931.

363 Rosi, A., Segoni, S., Catani, F., and Casagli, N.: Statistical and environmental analyses for the definition of a regional rainfall  
364 thresholds system for landslide triggering in Tuscany (Italy), *J. Geogr. Sci.*, 22, 617–629, 2012.

365 Rossi, G., Catani, F., Leoni, L., Segoni, S., and Tofani, V.: HIRESSS: a physically based slope stability simulator for HPC  
366 applications, *Nat. Hazards Earth Syst. Sci.*, 13, 151–166, doi:10.5194/nhess-13-151-2013, 2013.

367 Salciarini, D., Tamagnini, C., Conversini, P., and Rapinesi, S.: Spatially distributed rainfall thresholds for the initiation of shallow  
368 landslides, *Nat. Hazards*, 61(1), 229–245, doi:10.1007/s11069-011-9739-2, 2012.

369 Salciarini, D., Fanelli, G., Tamagnini, C.: A probabilistic model for rainfall-induced shallow landslide prediction at the regional  
370 scale, *Landslides*, 14(5), 1731–1746, 2017.

371 Simoni, S., Zanotti, F., Bertoldi, G., and Rigon, R.: Modelling the probability of occurrence of shallow landslides and channelized  
372 debris flows using GEOTop-FS, *Hydrolog. Process.*, 22, 532–545, 2008.

373 Tofani, V., Bicocchi, G., Rossi, G., Segoni, S., D'Ambrosio, M., Casagli, N., and Catani, F.: Soil characterization for shallow  
374 landslides modeling: a case study in the Northern Apennines (Central Italy), *Landslides*, 14, 755–770, doi: 10.1007/s10346-017-  
375 0809-8, 2017.

376 Thiery, Y., Vandromme, R., Maquaire, O., Berneradié, S.: Landslide susceptibility assessment by EPBM (Expert physically based  
377 model): strategy of calibration in complex environment. In: Mikoš, M., Tiwari, B., Yin, Y., Sassa, K. (Eds) *Advancing Culture of*  
378 *Living with Landslides. Proceedings, 2: Advances in Landslide Science*, Springer, 4th World Landslide Forum in Ljubljana, 917–  
379 926, doi: 10.1007/978-3-319-53498-5\_104, 2017.

380 Vergani, C., Bassanelli, C., Rossi, L., Chiaradia, E. A., and Bischetti, G. B.: The effect of chestnut coppice forest abandon on slope  
381 stability: a case study, *Geophys. Res Abstr*, 15, EGU2013-10151, 2013.

382 Vergani, C., Giadrossich, F., Schwarz, M., Buckley, P., Conedera, M., Pividori, M., Salbitano, F., Rauch, H. S., and Lovreglio, R.:  
383 Root reinforcement dynamics of European coppice woodlands and their effect on shallow landslides, a review *Earth Sci. Rev.*, 167,  
384 88–102, doi:10.1016/j.earscirev.2017.02.002, 2017.

385 Wagner, A. A.: The use of the Unified Soil Classification System by the Bureau of Reclamation, *Proc. 4th Intern. Conf. Soil Mech.*  
386 *Found. Eng.*, London, 1, 125, 1957.

387 Waldron, L. J., and Dakessian, S.: Soil reinforcement by roots: calculations of increased soil shear resistance from root properties,  
388 *Soil Sci.*, 132, 427–435, 1981.

**Table 1.** Geotechnical properties of survey points (grain size distribution, Atterberg limits, index properties, permeability and shear strength parameters).

<i>SITE</i>	<i>SOIL TYPE</i>	<i>G %</i>	<i>S %</i>	<i>M %</i>	<i>C %</i>	<i>LL (%)</i>	<i>PL (%)</i>	<i>PI (%)</i>	<i>USCS</i>	$\gamma$ ( <i>kN m<sup>-3</sup></i> )	$\gamma_d$ ( <i>kN m<sup>-3</sup></i> )	$\gamma_{sat}$ ( <i>kN m<sup>-3</sup></i> )	<i>n (%)</i>	<i>w (%)</i>	<i>k<sub>s</sub> (m s<sup>-1</sup>)</i>	<i>k<sub>sc</sub> (m s<sup>-1</sup>)</i>	$\phi'$ lab (°)	<i>c'</i> ( <i>kPa</i> )
<i>Site 1</i>	Sand with silty gravel	27.8	45.2	23.4	3.6	36	25	11	SM	16.7	13.7	18.3	47.3	11.3	/	2.52E-06	25.6	1.0
<i>Site 2</i>	Sand with gravelly silt	19.4	50.5	29.0	1.1	38	25	14	SC	19.1	14.5	18.8	44.3	11.4	2.71E-06	1.48E-06	34.3	1.5
<i>Site 3</i>	Sand with gravel and silt	26.9	45.2	26.8	1.1	/	/	/	/	/	/	/	/	/	/	8.89E-07	/	/
<i>Site 4</i>	Sand with gravelly silt	18.8	40.4	39.2	1.6	38	27	11	SM	19.5	14.8	19.0	43.2	10.7	1.36E-07	4.51E-07	34.3	0.0
<i>Site 5</i>	Sand with gravel and silt	31.0	43.1	25.7	0.2	47	36	11	SM	18.4	14.0	18.5	46.3	11.0	/	2.44E-06	25.7	9.3
<i>Site 6</i>	Sand with poorly silty gravel	28.5	57.5	13.9	0.1	52	38	13	SM	18.7	13.5	18.2	47.9	20.0	/	8.27E-06	30.2	4.4
<i>Site 7</i>	Sand with silty gravel	37.0	42.6	17.9	2.5	40	32	8	SM	20.3	15.5	19.5	40.4	26.2	5.18E-06	2.97E-06	28.2	3.4
<i>Site 8</i>	Sandy silty gravel	58.1	24.6	16.0	1.3	43	28	16	GM	17.2	15.7	19.6	39.6	9.4	/	3.76E-06	30.1	8.1
<i>Site 9</i>	Gravelly silty sand	18.7	55.1	24.4	1.8	46	36	10	SM	20.1	18.7	21.5	27.9	8.1	2.41E-06	1.73E-06	33.9	0.6
<i>Site 10</i>	Sand with gravelly silt	21.9	52.0	25.1	1	46	37	8	SM	18.4	16.0	19.8	38.6	15.5	/	2.10E-06	30.3	1.5
<i>Site 11</i>	Gravelly silty sand	24.3	51.4	21.2	3.1	31	25	7	SM	21.7	18.0	21.2	31.9	20.5	4.03E-06	3.05E-06	29.8	2.0
<i>Site 12</i>	Gravel with poorly silty sand	55.2	32.2	12.2	0.4	55	45	10	SM	15.3	14.6	18.9	43.9	5.1	1.54E-05	8.25E-06	30.2	1.6
	MEAN	30.63	44.98	22.9	1.48	42.91	32.18	10.82		18.67	15.36	19.39	41.03	13.56	4.98E-06	3.16E-06	30.24	3.04
	MEDIAN	27.35	45.2	23.9	1.2	43	32	11		18.7	14.8	19.0	43.2	11.3	3.37E-06	2.48E-06	30.2	1.6
	STD.DEV	13.31	9.48	7.41	1.11	7.15	6.71	2.71	/	1.80	1.68	1.10	6.34	6.30	5.38E-06	2.56E-06	3.05	3.07
	MAX	58.1	57.5	39.2	3.6	55	45	16		21.7	18.7	21.5	47.9	26.2	1.54E-05	8.27E-06	34.3	9.3
	MIN	18.7	24.6	12.2	0.1	31	25	7		15.3	13.5	18.2	27.9	5.1	1.36E-07	4.51E-07	25.6	0

**Table 2.** Spatialized geotechnical parameters of each lithological class as input for HIRESSS model.

<i>Lithological classes</i>	<i>Soil Type</i>	$\phi' \text{ lab } (^{\circ})$	$c' \text{ (Pa)}$	$\gamma_d \text{ (kN m}^{-3}\text{)}$	$n \text{ (\%)}$	$k_s \text{ (m s}^{-1}\text{)}$	$h_s$	$q_r$	$l$
Calcareous schist	Sand with gravelly silt	31	1000	16.5	39	1.1E-05	0.1466	0.041	0.322
Alluvial deposits	Sand with gravel and silt	26	1000	14.0	46	3.0E-06	0.1466	0.041	0.322
Glacial deposits	Sand with silty gravel	31	1000	15.3	41	2.7E-06	0.1466	0.041	0.322
Colluvial deposits	Sand with silty gravel	25	1000	13.7	47	2.5E-06	0.1466	0.041	0.322
Granites	Sandy gravel	30	1000	17.6	32	4.0E-06	0.1466	0.041	0.322
Mica schists	Sandy silty gravel	30	1000	17.7	32	6.0E-06	0.1466	0.041	0.322
Green stones	Gravel with silty sand	32	1000	16.3	37	4.6E-06	0.1466	0.041	0.322

**Table 3.** Main characteristics of the simulation.

	2008 event	2009 event
Spatial resolution	10 m	10 m
Time step	1h	1h
Rainfall hours	192	96

5 **Table 4.** Hiresss results over 75% of slope failure probability for two events.

<b>Event 2008</b>	<b>N. Pixel</b>	<b>Total %</b>	<b>Pixel area (km<sup>2</sup>)</b>
24/05/2008	62344	1	6
25/05/2008	21295	0	2
26/05/2008	84256	1	8
27/05/2008	95220	1	10
28/05/2008	15364	0	2
29/05/2008	243137	3	24
30/05/2008	79437	1	8
31/05/2008	7110	0	1
<b>Event 2009</b>	<b>N. Pixel</b>	<b>Total %</b>	<b>Pixel area (km<sup>2</sup>)</b>
25/04/2009	0	0	0
26/04/2009	52644	1	5
27/04/2009	326826	4	33
28/04/2009	56599	1	6

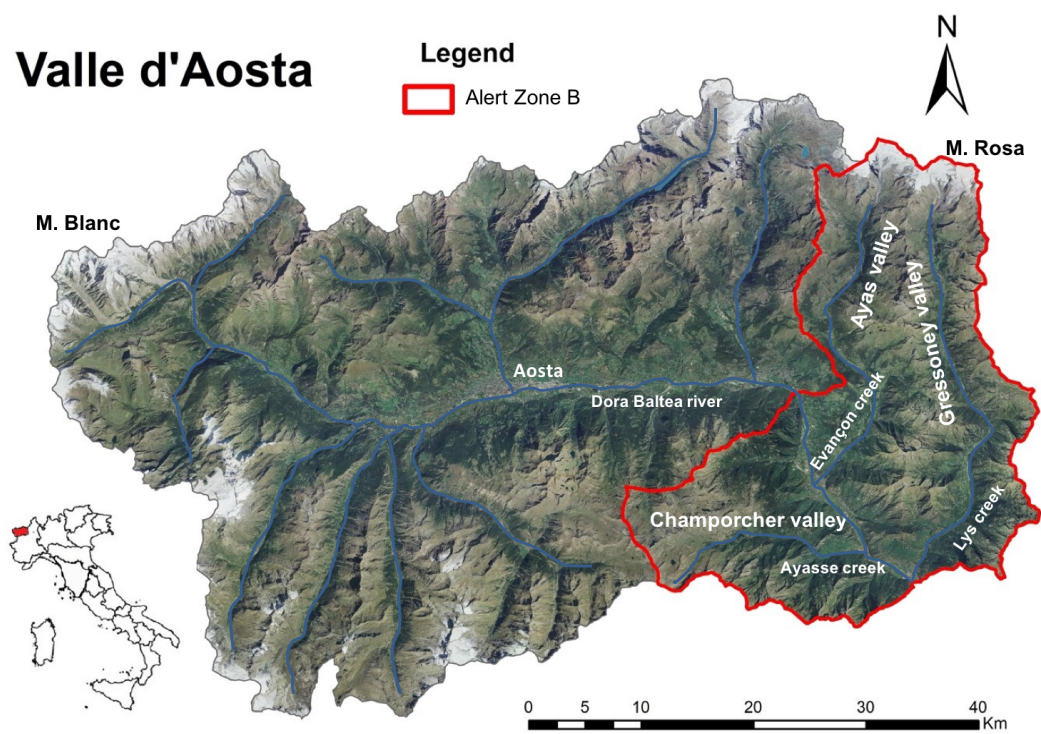


**Figure 1.** Valle d'Aosta region in the NW Italy: in red the study area, alert Zone B.

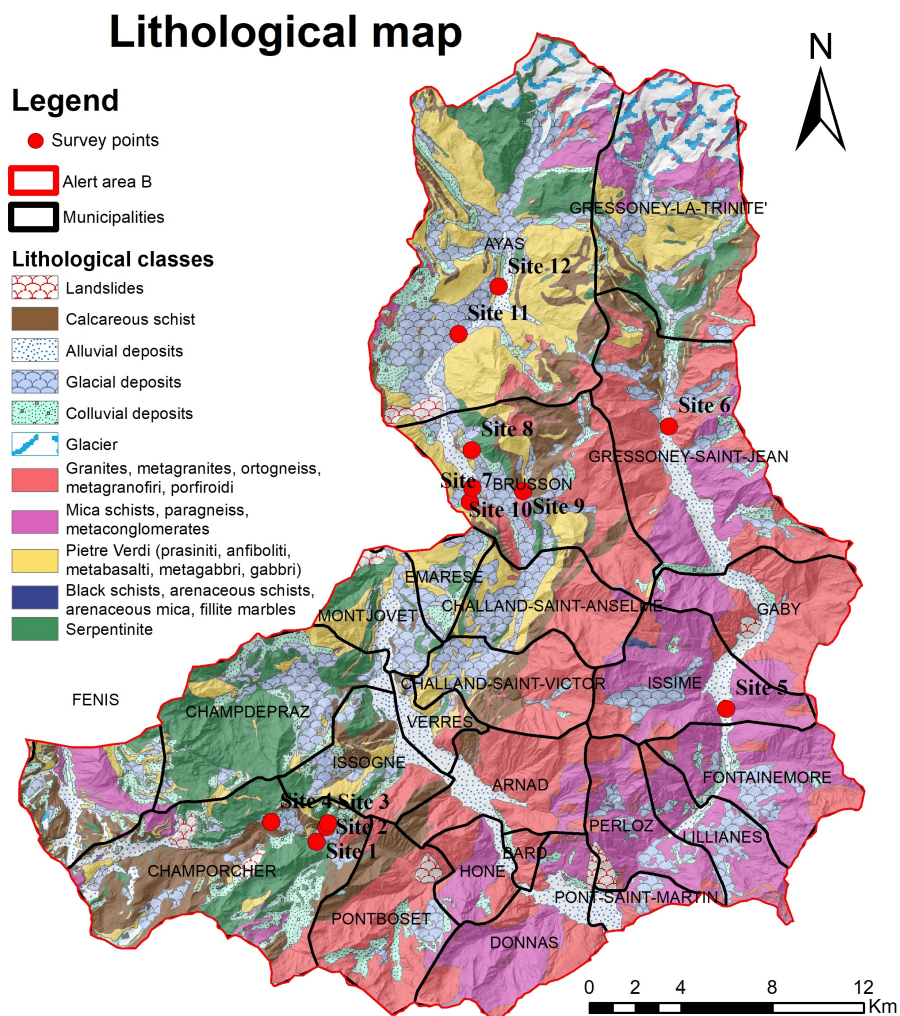


**Figure 2.** Spatial distribution of survey points compared to the geo-lithology.



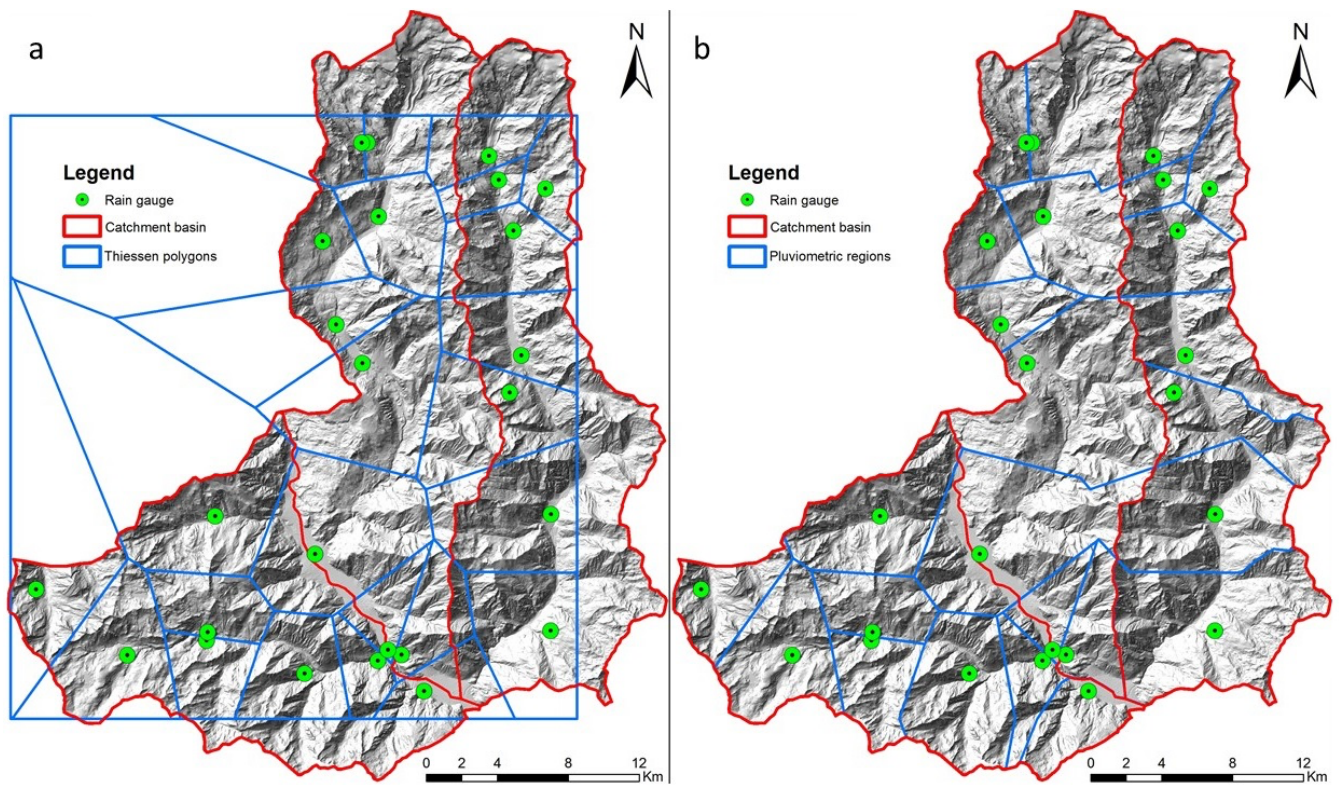
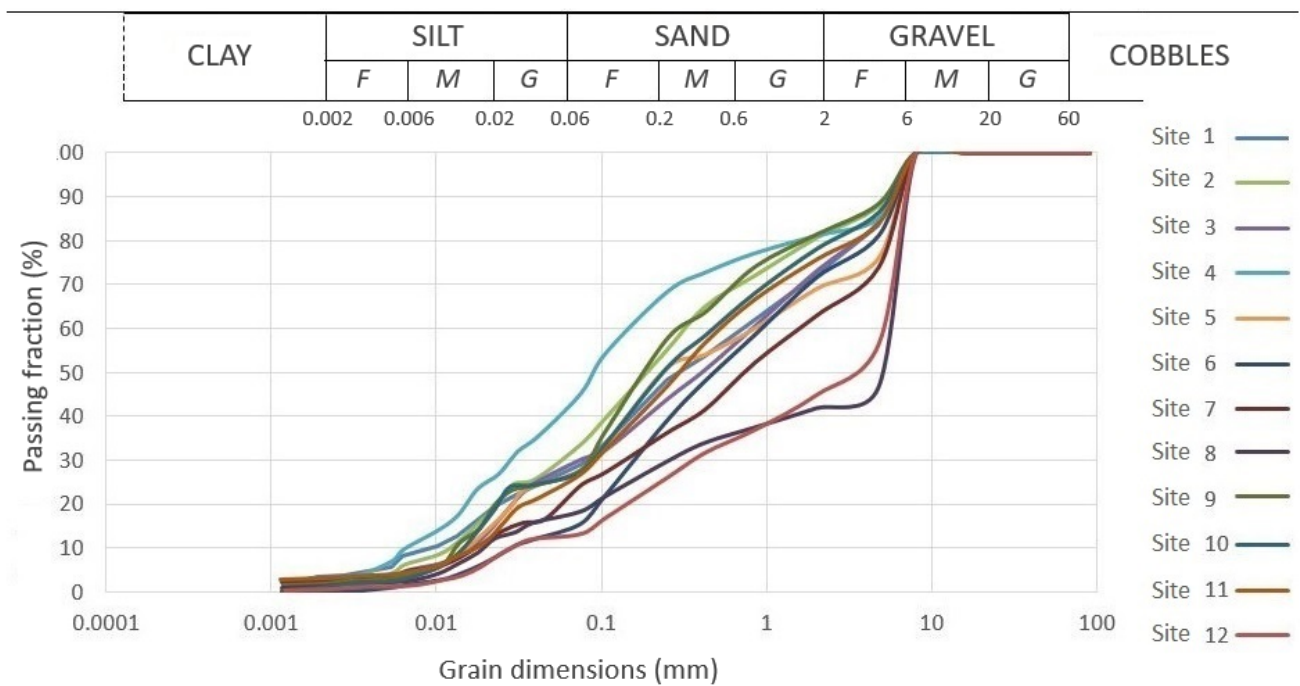


**Figure 3.** Comparison of Thiessen's polygons methodology a) simple b) modified according to the catchment basins boundaries.



5 **Figure 4.** Grain size distributions of soil samples.



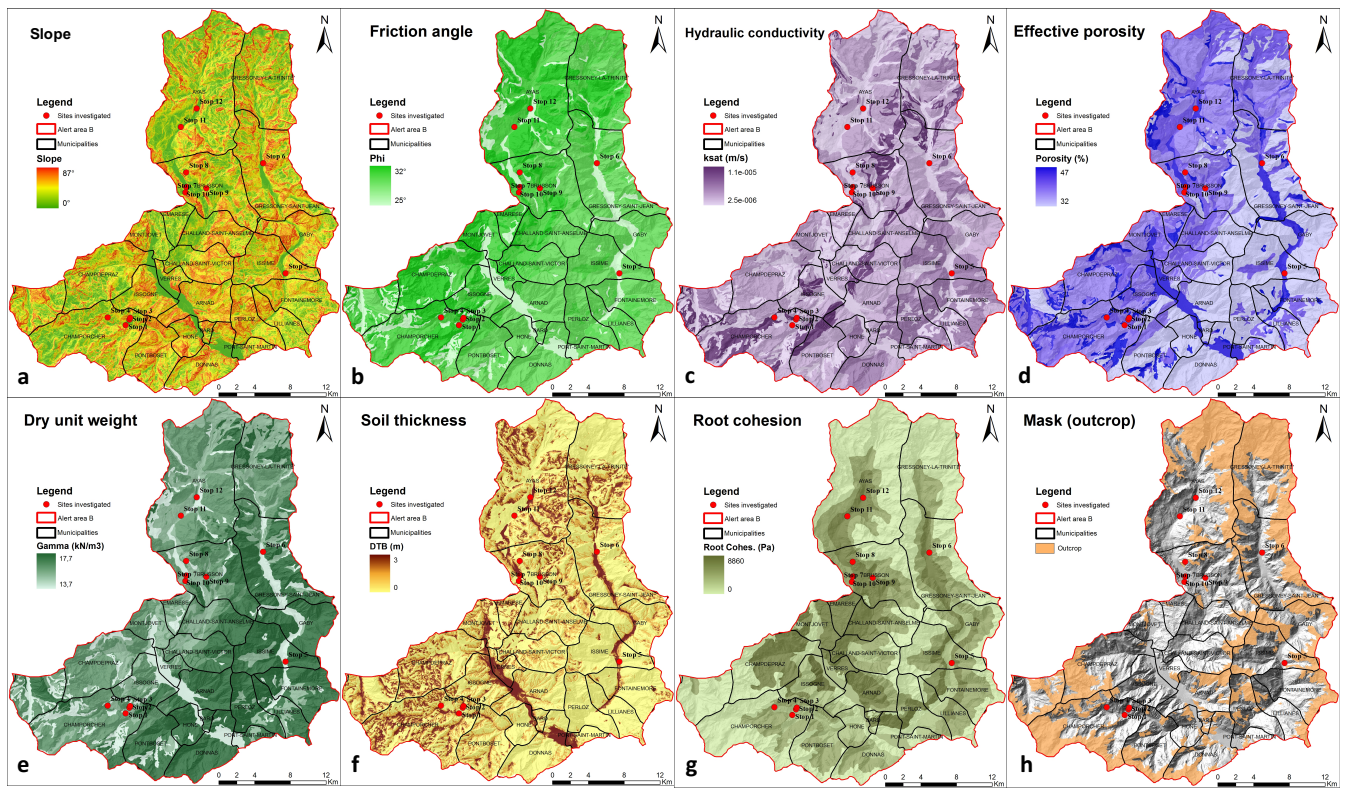


**Figure 5.** Static input parameters for HIRESSS model, a) slope gradient; b) friction angle; c) Hydraulic conductivity; d) effective porosity; e) dry unit weight; f) soil thickness; g) root cohesion; and h) exposure rock mask.

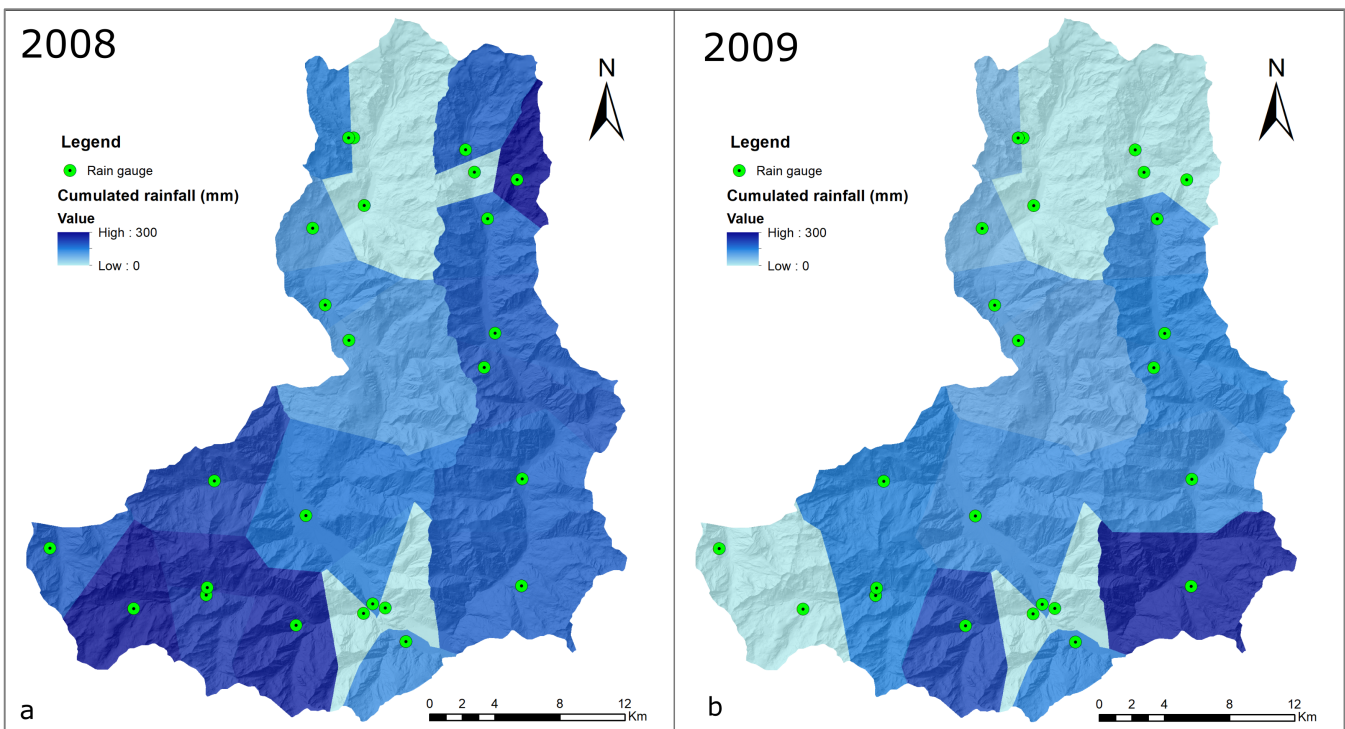


**Figure 6.** Cumulated rainfall maps for two events.

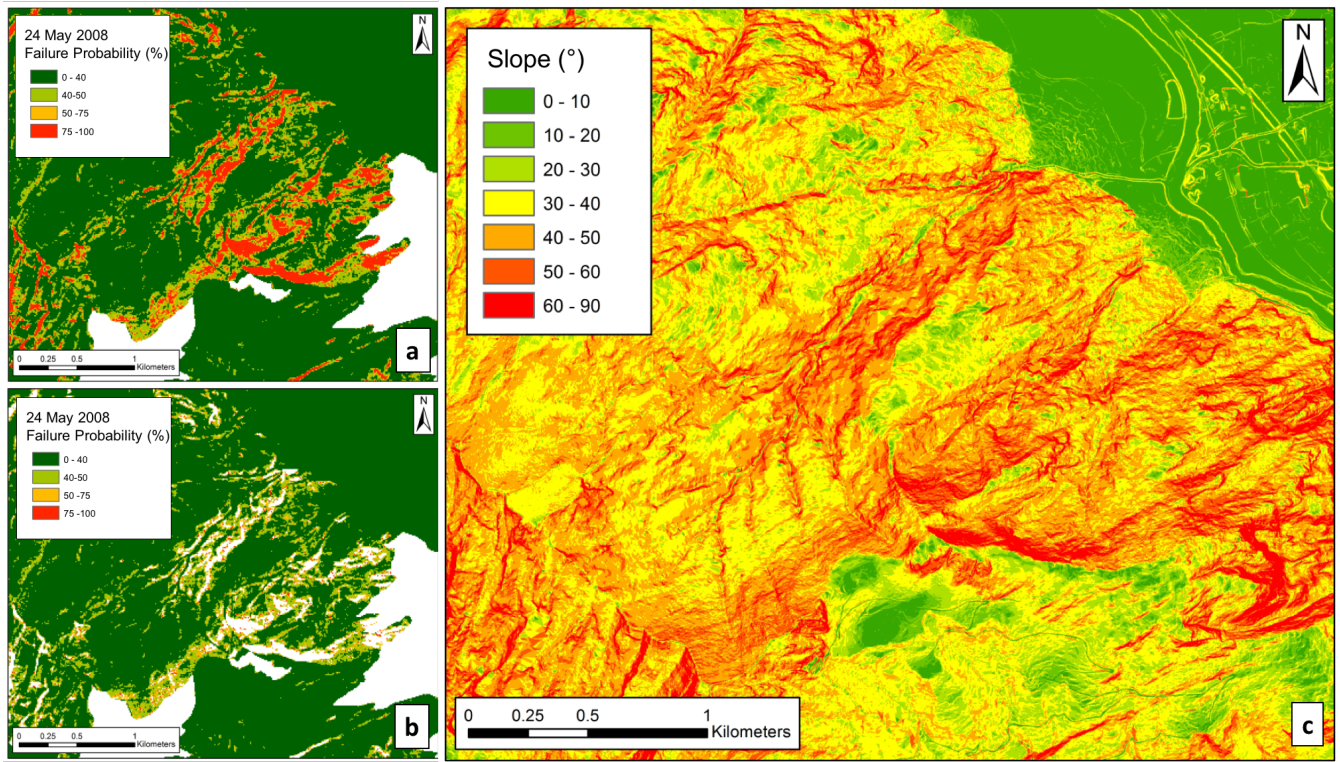


**Figure 7.** Example of numerical mask to remove the false positive of the first event simulated, between 24-31 May 2008, a) the HIRESSES result of the first day of simulation with false positive pixels, b) the probability map after the numerical mask implementation, c) the slope map shows that the pixels with high probability of landslide occurrence are located where the slope is higher than 60%.



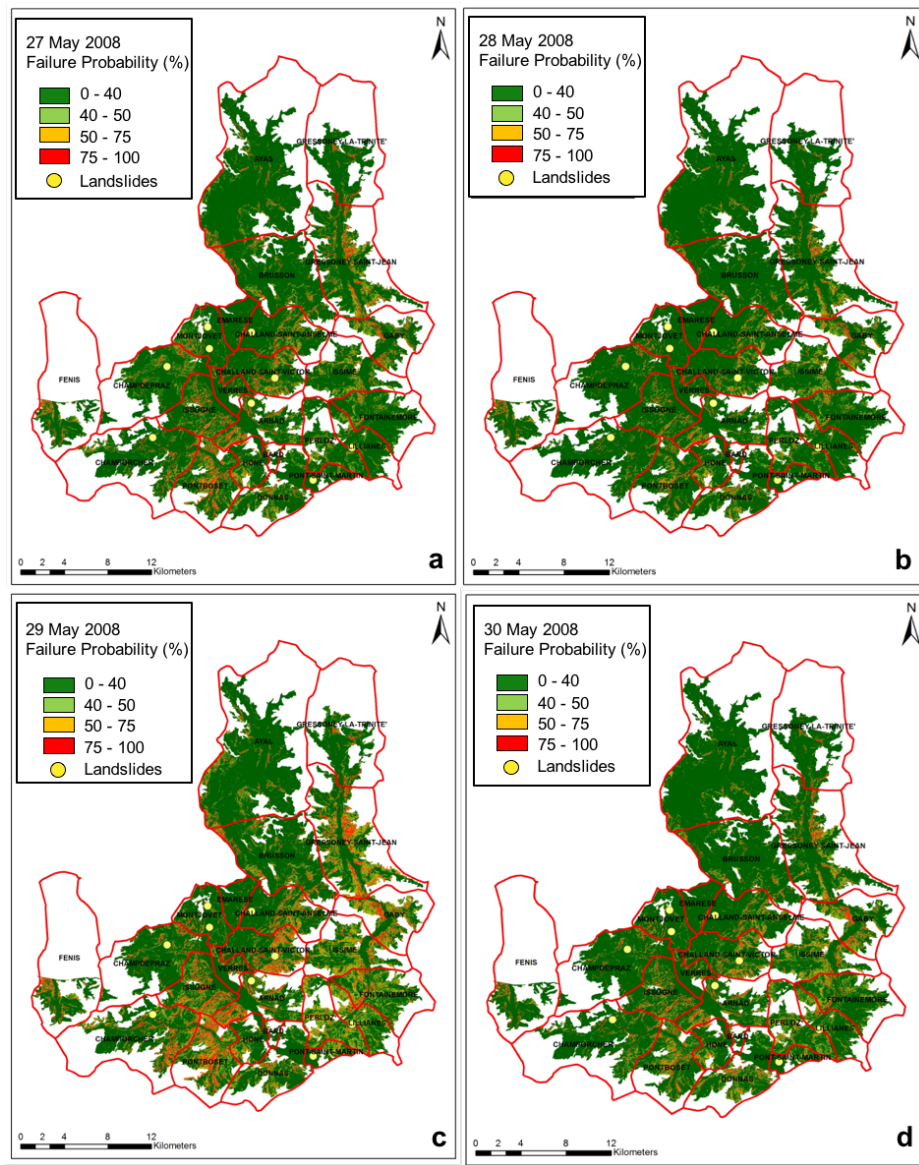


**Figure 8.** HIRESSES landslide probability maps of simulate event of 24-31 May 2008 and reporting landslide during this event focused on the four critical days, a) 27 May 2008, b) 28 May 2008, c) 29 May 2008, and d) 30 May 2008.

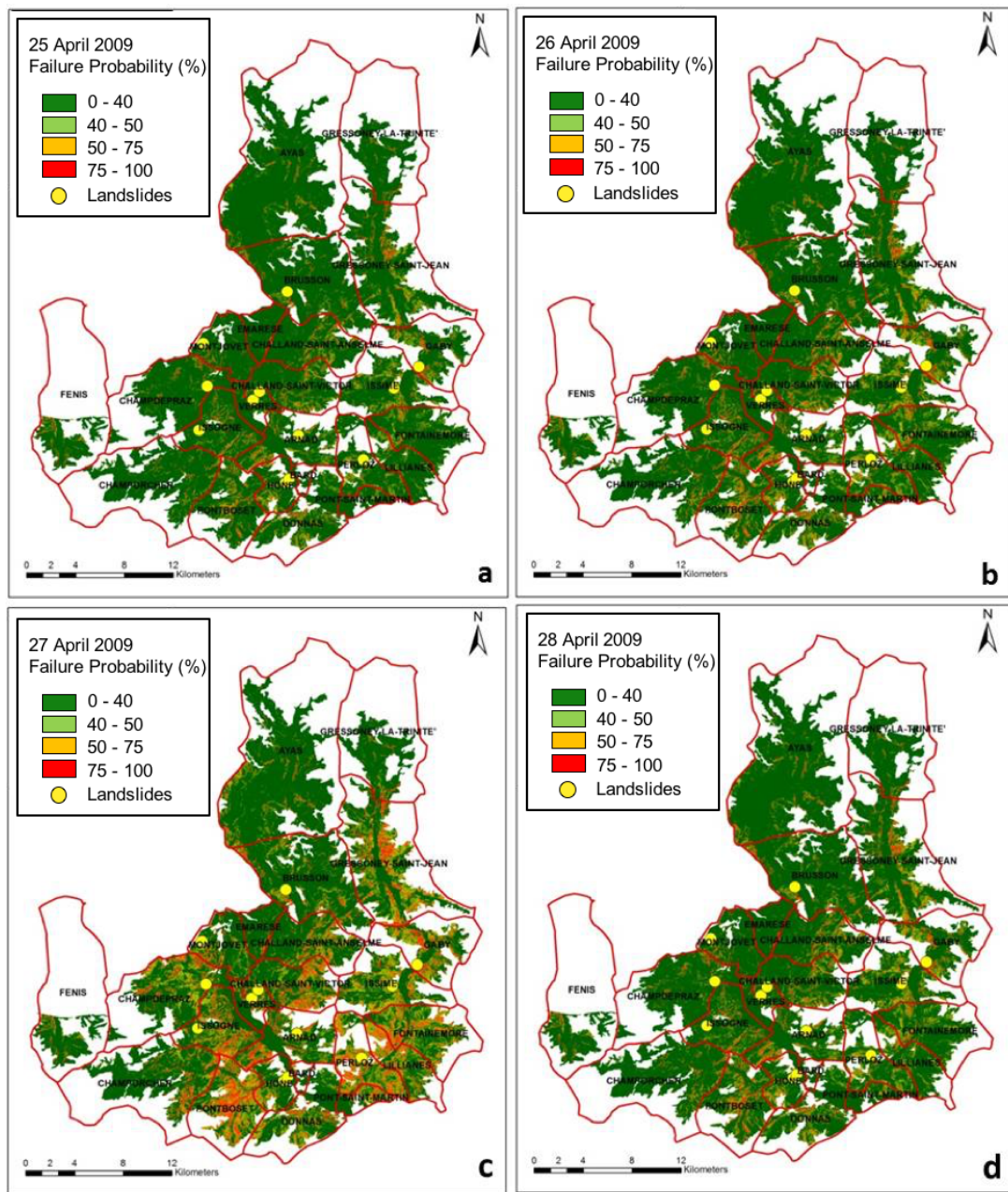


**Figure 9.** HIRESSE landslide probability maps of simulate event between 25 - 28 April 2009 and reporting landslide during this event, a) 25 April 2009, b) 26 April 2009, c) 27 April 2009 and d) 28 April, 2009.

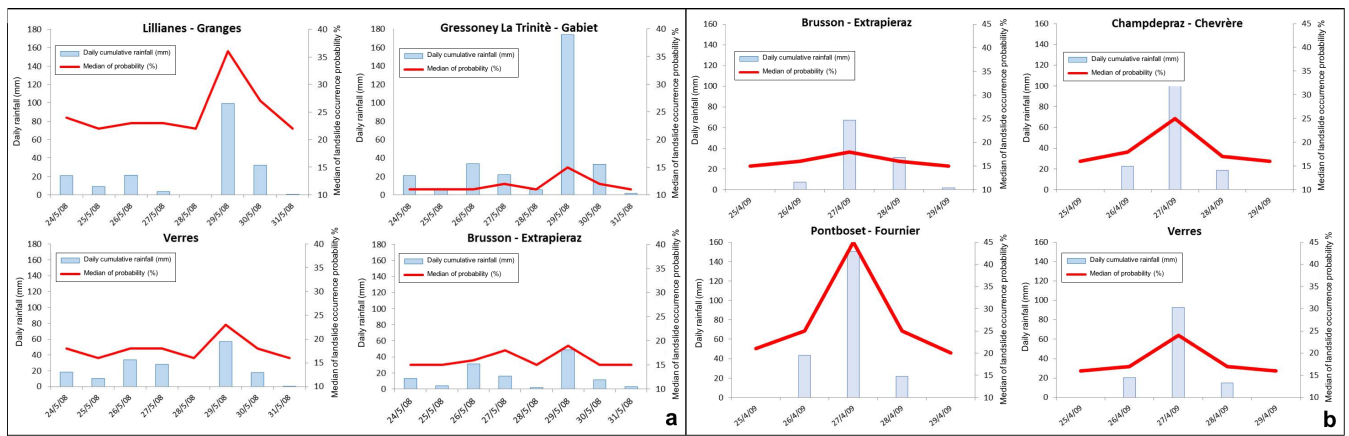


**Figure 10.** Correlation graphs between the daily cumulative rainfall and the median of landslide occurrence probability for both events.

5

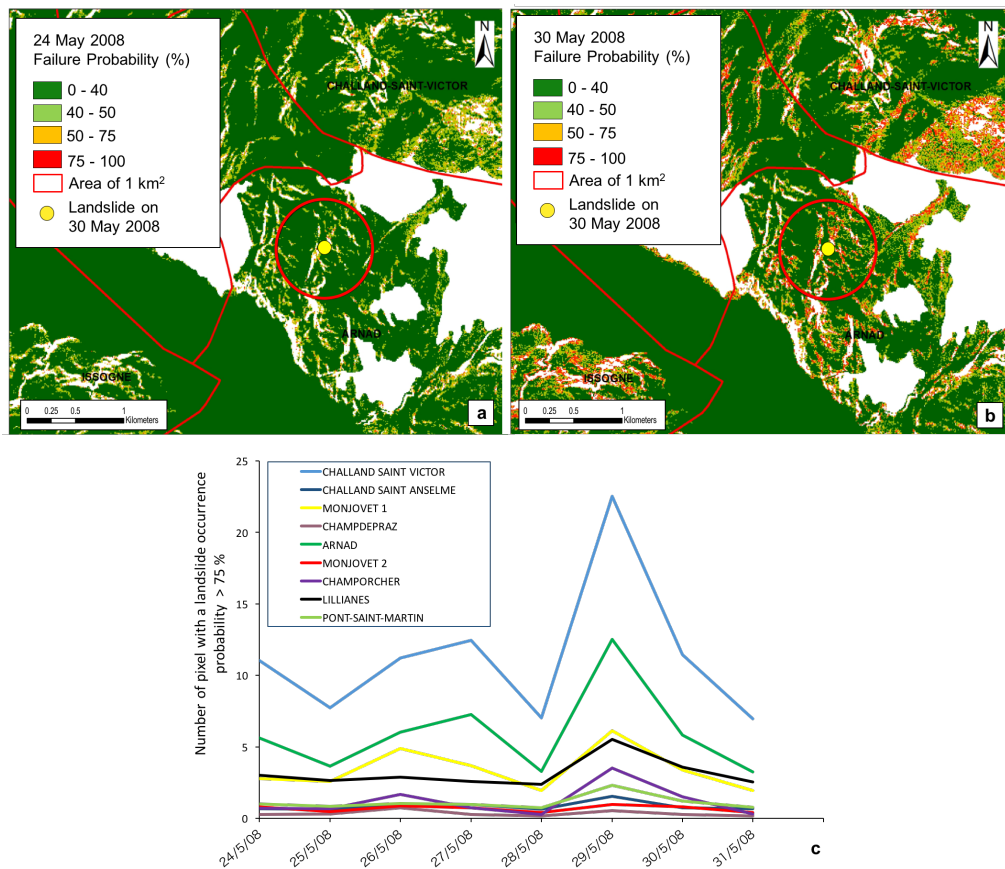


**Figure 11.** An example of landslide event happened in the Arnad municipality compared to landslide occurrence probability map, a) before and b) after rainfall event. c) Number of pixels above 75% of probability calculated by the model for all the landslides triggered during the event in the study area.

10